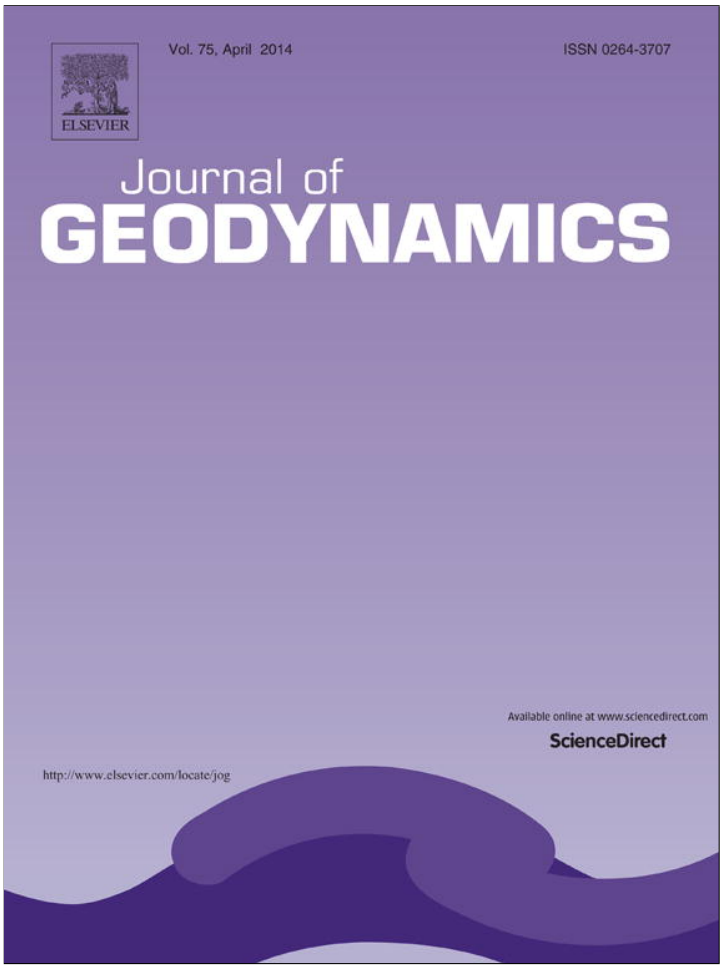

Journal of Geodynamics 75 (2014) 1–8

Contents lists available at ScienceDirect

Journal of Geodynamics

journal homepage: http://www.elsevier.com/locate/jog

Kinematic model of crustal deformation of Fenwei basin, China based on GPS observations

Wei Qu[a], Zhong Lu[b,*], Qin Zhang[a], Zhenhong Li[c], Jianbin Peng[a], Qingliang Wang[d], Jane Drummond[c], Ming Zhang[a]

[a] College of Geology Engineering and Geomatics, Chang'an University, Xian, Shaanxi, China
[b] Department of Earth Sciences, Southern Methodist University, Dallas, TX, USA
[c] School of Geographical and Earth Sciences, University of Glasgow, UK
[d] Second Monitoring and Application Center, CEA, Xian, Shaanxi, China

ARTICLE INFO

Article history:
Received 17 April 2013
Received in revised form
31 December 2013
Accepted 2 January 2014
Available online 9 January 2014

Keywords:
Block kinematic models
Fenwei basin
GPS
Crustal deformation
Hypothesis testing

ABSTRACT

Using high precision GPS data for the period of 1999–2007 from the China Crustal Movement Observation Network, we have constructed a plate kinematic model of crustal deformation of Fenwei basin, China. We have examined different kinematic models that can fit the horizontal crustal deformation of the Fenwei basin using three steps of testing. The first step is to carry out unbiasedness and efficiency tests of various models. The second step is to conduct significance tests of strain parameters of the models. The third step is to examine whether strain parameters can fully represent the deformation characteristics of the 11 tectonic blocks over the Fenwei basin. Our results show that the degree of rigidity at the Ordos, Hetao, Yinshan and South China blocks is significant at the 95% confidence level, indicating the crustal deformation of these blocks can be represented by a rigid block model without the need to consider differential deformation within blocks. We have demonstrated that homogeneous strain condition is suitable for the Yinchuan basin but not for other 6 blocks. Therefore, inhomogeneous strains within blocks should be considered when establishing the crustal deformation model for these blocks. We have also tested that not all of the quadratic terms of strain parameters are needed for the Yuncheng-Linfen block. Therefore, four kinds of elastic kinematic models that can best represent the detailed deformation characteristics of the 11 blocks of Fenwei basin are finally obtained. Based on the established model, we have shown that the current tectonic strain feature of the Fenwei basin is mainly characterized by tensile strain in the NW–SE direction, and the boundaries betweem the Ganqing and Ordos blocks and the Shanxi graben possess the maximum shear strain. A comparison between our results and past geological and geophysical investigations further confirms that the model established in this paper is reasonable.

1. Introduction

The discovery of plate tectonics theory and subsequent studies on plate kinematic models have made enormous contributions to the understanding of global and regional plate deformation, lithosphere geodynamics, and the development of geosciences (McKenzie, 1972; Dewey et al., 1973). Based on geological, geophysical and geodetic investigations, various kinematic models have been established, including REVEL 2000 (Sella et al., 2002), CGPS 2004 (Prawirodirdjo and Bock, 2004), APKM 2005 (Drewes, 2009), MORVEL 2010 (DeMets et al., 2010), GEODVEL 2010 (Argus et al., 2010), NNR-MORVEL56 (Argus et al., 2011), and others (Zhang et al., 1999; Fu et al., 2002; Burbidge, 2004; Nanjo et al., 2005; Wu et al., 2006). Therefore, the tectonic deformation within plates and at their boundaries can be monitored at an accuracy of millimeters.

For satellite observations on time scales from years to decades, the deformation within a plate is mainly characterized as elastic and the plate can be treated as an elastic medium (Reynolds et al., 2002; Teng, 2003; Li et al., 2007).

In this paper, we select the Fenwei basin as our study area (Fig. 1). It is situated in the middle of China. It is about several hundred kilometers long and appears as an "S" in shape. Fenwei basin represents a deep rift that divides China into eastern and western parts. Bounded by the Ordos, North China and South China blocks, Fenwei basin is not only the accommodation zone of differential motions of these three blocks, but also the border and decoupled strip of tectonics between western and eastern China (Fan et al., 2003; Dai et al., 2004).

The Ordos, North China and South China blocks surrounding the Fenwei basin have different patterns (directions and magnitudes)

* Corresponding author. Tel.: +1 214 768 0101; fax: +1 214 768 4291.
E-mail addresses: zhonglu@smu.edu, insar_fringes@yahoo.com (Z. Lu).

0264-3707/$ – see front matter © 2014 Elsevier Ltd. All rights reserved.
http://dx.doi.org/10.1016/j.jog.2014.01.001

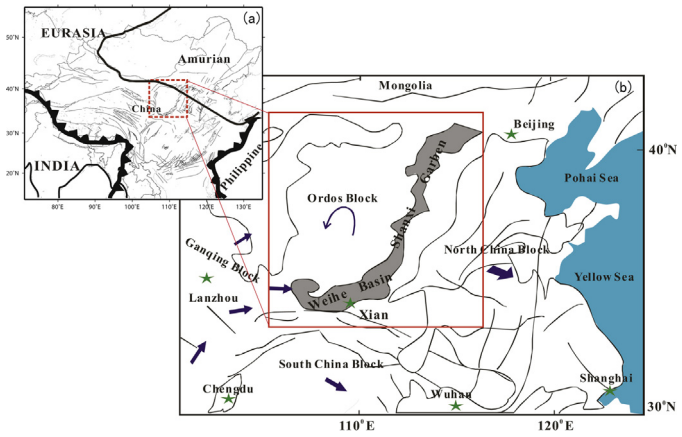

Fig. 1. Location of Fenwei basin in China. The red rectangular box outlines the study area and the "S" shape with gray color represents the Fenwei basin. The Fenwei basin is composed of Weihe basin (southern part) and Shanxi graben (northern part). From south to north, the Shanxi graben can be segmented into Yuncheng-Linfen, Taiyuan-Xinzhou and Datong basins (details shown in Fig. 2). The thin blue arrow denotes the motion characteristic of the Ordos block while thick black arrows represent the motion directions of major microplates in China, such as the North China block, South China block and Ganqing block. Stars denote main cities in China, such as Beijing, Shanghai, Xi'an, Chengdu, Wuhan and Lanzhou. Solid lines represent main faults in China. The inset over the upperleft corner shows the map of China and the location of our study area. (For interpretation of the references to color in this figure legend, the reader is referred to the web version of the article.)

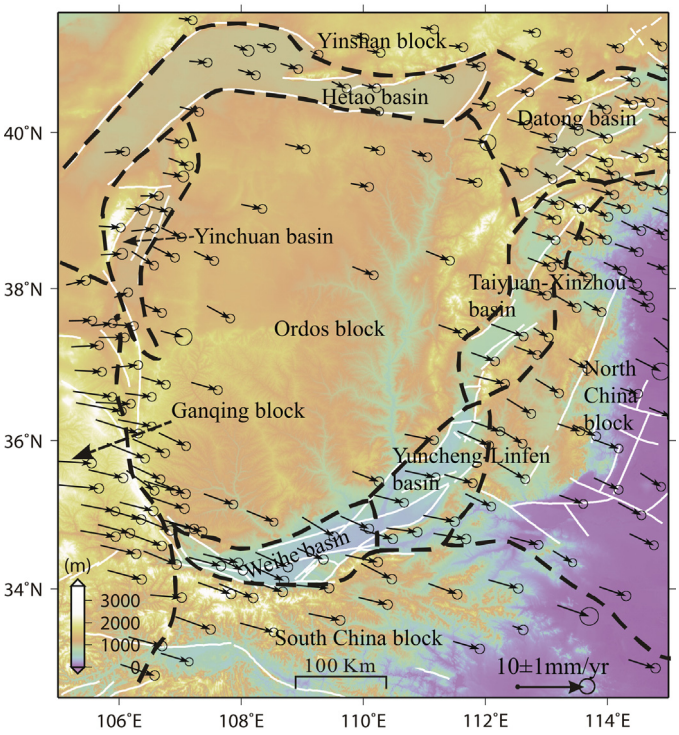

Fig. 2. GPS velocities in the Fenwei basin and its surrounding blocks for the period of 1999–2007. Solid arrows are observed GPS velocities with respect to the stable Eurasia plate based on ITRF2005 reference frame. Each arrow originates at the location of the station and points to its motion direction. The error ellipse represent the 95% confidence limit. The white stripes represent main faults over the region (Zhang et al., 2005). There are a total of 11 blocks.

of deformation, so the basin is significantly influenced by motions of those three blocks. Furthermore, geological features and tectonic setting within the basin are relatively complicated. The Fenwei basin comprised a series of active blocks: Weihe basin in the south and Shanxi graben in the north. From south to north, the Shanxi graben can be segmented into Yuncheng-Linfen, Taiyuan-Xinzhou and Datong Basins. Because active blocks within Fenwei basin have different geographic positions and geological backgrounds, they possess different crustal deformation characteristics. These result in intense crustal movements and frequent geological disasters in the Fenwei basin such as earthquakes disasters and ground fissures (Jiang et al., 2000; Myers and Gomez, 2010; Zhang et al., 2011).

Several studies have been conducted regarding the tectonics of Fenwei basin and its surrounding regions. Fault activities and large earthquakes in history around Ordos block were investigated (Jiang et al., 2000; Fan et al., 2003; Dai et al., 2004; Li et al., 2008; Yang et al., 2013). Present-day crustal movement and tectonic deformation of Ordos block and its surroundings were studied based on GPS observations (Shen et al., 2000; Wang et al., 2002; Lin et al., 2013). The evolution of tectonic stress from the Cenozoic to present was obtained by numerical simulation and geophysical/geological investigations (Zhang et al., 2011, 2003; Wang et al., 2012). In addition, mantle anisotropy results beneath the study area were obtained by tomography mapping (Huang and Zhao, 2006; Chang et al., 2007; Tang et al., 2010; Tian et al., 2011).

However, previous studies applied geophysical and geological methods to investigate faults, seismic activities, or geophysical characteristics of the study area, where GPS data were only used to describe the crustal motion. In this paper, using 1999–2007 GPS data from the China Crustal Movement Observation Network (CCMON) we attempt to establish the present-day plate kinematic model of the region. We conduct a series of procedures to ensure that the model reflects the deformation characteristics of the region revealed by the GPS data. Because models with slightly different strain parameters might fit the same observed deformation data, we need carry out vigorous statistical tests regarding the validity, applicability, and reasonability of models in order to derive the best kinematic model that represents the contemporary crustal deformation feature of the area.

2. GPS data and the division of active blocks

GPS data used in this study were from 224 GPS sites of the China Crustal Movement Observation Network (CCMON) project, including 2 continuous stations from China GPS fiducial network observed during 1998–2007, 7 survey-mode sites that were occupied annually during 1998–2007, and 215 survey-mode stations that were surveyed in 1999, 2001, 2004 and 2007. All GPS sites are located on stable bedrocks, and all survey-mode sites were observed continuously for at least 4 days during each survey.

The GPS velocities (Fig. 2) used in the study were taken from Wang et al. (2010), who adopted the GPS processing strategy used in Shen et al. (2000) for data analysis. The GPS carrier phase data were processed using GAMIT/GLOBK software (King and Bock, 2000; Herring, 2002). Station positions and velocities were estimated through a Kalman filter procedure using QOCA software (http://gipsy.jpl.nasa.gov/qoca/). The velocity solution was with respect to the global reference frame ITRF2005 (Altamimi et al., 2007). Further, in order to characterize the crustal movement inside China, the velocity field was transformed into a regional reference frame with respect to the Eurasian plate by applying constraints that minimize the motions at 11 IGS stations distributed within the stable plate interiors: NYAL (Norway), ONSA (Sweden), POTS (Germany), HERS (United Kingdom), WSRT and KOSG (Holland), WTZR (Germany), VILL (Spain), GLSV (Ukraine), and IRKT and TIXI (Siberia).

It can be seen from Fig. 2 that the whole area has an overall tendency of moving toward the SE direction and the GPS velocity over the western and southern parts of the study area is relatively

larger than that of the eastern and northern parts. It can also be observed that the Fenwei basin is divided into a number of tectonic systems (blocks and basins) sewed by deep fractures. It has been shown that the difference in tectonic deformation exists not only within the Fenwei basin but also in the surrounding blocks, each of which possess different deformation characteristics (Fan et al., 2003). Furthermore, the tectonic activities of different segments (Fig. 1) within the Shanxi graben are diverse (Fan et al., 2003).

In this paper, the Fenwei basin and its surroundings are regarded as an integrated tectonic system comprised blocks (and basins) with different activities. Therefore, we make use of block kinematic models to study the present crustal tectonic deformation characteristics of the whole region. Accordingly, we first divide the whole region into a number of blocks. Based on the division results for the mainland of China and second-tier activity blocks provided by Zhang et al. (2005), combined with the geological structure, earthquake distribution and the distribution of late Quaternary rifts, the whole region was divided into 11 blocks (Fig. 2). They are the Yinshan block, South China block, North China block, Ordos block and Ganqing block (in the eastern margin of Tibet); and the Hetao basin, Yinchuan basin, Weihe basin, Yuncheng-Linfen basin, Taiyuan-Xinzhou basin and Datong basin.

3. Establishment of block kinematic models

In the traditional theory of plate tectonics, a block is considered as a rigid body. According to the Euler theorem for a rigid block, the block kinematic model can be defined by the following equation:

$$\begin{bmatrix} V_e \\ V_n \end{bmatrix} = r \begin{bmatrix} -\sin\varphi\cos\lambda & -\sin\varphi\sin\lambda & \cos\varphi \\ \sin\lambda & -\cos\lambda & 0 \end{bmatrix} \begin{bmatrix} \omega_x \\ \omega_y \\ \omega_z \end{bmatrix} \quad (1)$$

where (λ, φ) are the longitude and latitude of any point within a block, V_e and V_n are the eastern and northern components of the velocity vector of the point, r is the Earth radius, and ω_x, ω_y, ω_z are the components of the Euler vector. Eq. (1) takes no account of the radial (vertical) deformation of the GPS sites because the radial deformation of the Fenwei basin and its surroundings is not significant (Fan et al., 2003).

However, many reports have demonstrated that some blocks are not purely rigid (Burbidge, 2004; Nanjo et al., 2005). Therefore, deformation exists not only over the boundary zones of the blocks but also within blocks. Hence, the crustal motion of any GPS point within a block is the superimpostion of the block rotation and the diffential deformation within the block. If the differential motion (or strain) within a block is homogeneous, the compound velocity vector of a point within a block can be described as follows:

$$\begin{bmatrix} V_e \\ V_n \end{bmatrix} = r \begin{bmatrix} -\sin\varphi\cos\lambda & -\sin\varphi\sin\lambda & \cos\varphi \\ \sin\lambda & -\cos\lambda & 0 \end{bmatrix} \begin{bmatrix} \omega_x \\ \omega_y \\ \omega_z \end{bmatrix} + \begin{bmatrix} \varepsilon_e & \varepsilon_{en} \\ \varepsilon_{en} & \varepsilon_n \end{bmatrix} \begin{bmatrix} x \\ y \end{bmatrix} \quad (2)$$

where ε_e, ε_{en}, ε_n represent homogeneous strain parameters which can be defined as:

$$\varepsilon_e = \frac{\partial u_e}{\partial(r\cos\varphi(\lambda-\lambda_0))}, \varepsilon_n = \frac{\partial u_n}{\partial(r(\varphi-\varphi_0))},$$
$$\varepsilon_{en} = \varepsilon_{ne} = \frac{1}{2}\left(\frac{\partial u_e}{\partial(r(\varphi-\varphi_0))} + \frac{\partial u_n}{\partial(r\cos\varphi(\lambda-\lambda_0))}\right) \quad (3)$$

where (λ_0, φ_0) are the longitude and latitude of the block center, $x = r\cos\varphi(\lambda-\lambda_0)$ and $y = r(\varphi-\varphi_0)$. We use the coordinates of GPS stations within a block to obtain the mean coordinates of stations, which are regarded as the coordinates of the block center. And u_e and u_n are displacements in the eastern and nothern components, respectively (Savage et al., 2001; Shi and Zhu, 2006).

Finally, if the strain is uneven within a block, there is a need to model the variable strain within the block. Then we can obtain the total motion of any point within a block by including the motion due to the rigid rotation and the motion due to the uneven strain within a block. The combined eqution can be described as follows (Li et al., 2007):

$$\begin{bmatrix} V_e \\ V_n \end{bmatrix} = \begin{bmatrix} -r\sin\varphi\cos\lambda & -r\sin\varphi\sin\lambda & r\cos\varphi \\ r\sin\lambda & -r\cos\lambda & 0 \end{bmatrix} \begin{bmatrix} \omega_x \\ \omega_y \\ \omega_z \end{bmatrix} + \begin{bmatrix} A_0 & B_0 \\ B_0 & C_0 \end{bmatrix} \begin{bmatrix} x \\ y \end{bmatrix} + \frac{1}{2}\begin{bmatrix} \xi_1 & \xi_2 \\ \zeta_1 & \zeta_2 \end{bmatrix} \begin{bmatrix} x^2 \\ y^2 \end{bmatrix} + \begin{bmatrix} \xi_3 \\ \zeta_3 \end{bmatrix} xy \quad (4)$$

where A_0, B_0, C_0, ξ_1, ξ_2, ξ_3, ζ_1, ζ_2, ζ_3 are the strain parameters. Eq. (4) is the elastic kinematic model that describes the combined effect of the rigid rotation and the spatially variable deformation within a block. The first term on the right side of Eq. (4) represents the rigid rotation component while the second to the fourth terms represent the variable deformation components within the block.

4. Establishment and hypothesis testing of regional kinematic models

4.1. Model unbiasedness and effectiveness tests

As the accuracy of parameter estimation is related to the accuracy of GPS observations, we have designed a scheme of station screening and parameter optimization. Using 2σ (standard deviation) of GPS velocity as the tolerance value, we remove outlier GPS stations whose absolute residuals between the measured and model-predicted velocities by Eq. (2) are greater than the tolerance value. Furthermore, the station screening and parameter optimization are done through iterative steps. The model parameters are reestimated after removing the largest residuals one by one. When residuals at all remaining GPS sites are equal to or less than the 2σ of GPS velocity, we complete the screening of GPS observations. The station outliers are randomly distributed near the boundaries among different blocks. According to this prcedure, we finally obtain 187 out of a total of 224 GPS stations.

According to statistics theory (Tao, 2007), we should first analyze the unbiasedness and effectiveness of models on the basis of the selected GPS observations, and then quantitatively evaluate whether the established rigid rotation and homogeneous strain model (Eq. (2)) is better than the rigid block model (Eq. (1)). According to the requirement of unbiasedness and optimization, the best model should possess the least absolute residual $\Delta\bar{v}$ and variance $S_{\Delta v}$:

$$\Delta\bar{v} = \frac{1}{2n}\left(\sum_{i=1}^{n}\Delta v_{ei} + \sum_{i=1}^{n}\Delta v_{ni}\right) \quad (5)$$

$$S_{\Delta v} = \left[\frac{1}{2n-R}\left(\sum_{i=1}^{n}\Delta v_{ei}^2 + \sum_{i=1}^{n}\Delta v_{ni}^2\right)\right]^{1/2} \quad (6)$$

where Δv_{ei} and Δv_{ni} are the residual (difference between the observed and model-predicted) velocity components of a GPS point in the eastern and northern directions; n is the number of GPS sta-

Table 1
F test results for the rigid block model (model A) and the overall rotation and homogeneous strain model (model B) of the Fenwei basin and its surrounding blocks at a reference critical value $\alpha = 0.05$.

Blocks (basins)	Model A	Model B	Model A	Model B	Model A		Model B		Testing	*F* test		Testing
	$\Delta\bar{v}$	$\Delta\bar{v}$	$S_{\Delta v}$	$S_{\Delta v}$	T	T_α	T	T_α		F	F_α	
Yinchuan	0.00940	−0.00272	0.603923	0.348978	0.066047	1.7531	0.033116	1.7823	Pass	0.417	2.62	Pass
Hetao	0.00049	−0.00004	0.500808	0.440020	0.004550	1.7291	0.000402	1.7459	Pass	0.917	2.28	Pass
Yinshan	−0.00021	−0.000003	0.121030	0.103654	0.007393	1.7531	0.000124	1.7823	Pass	0.917	2.62	Pass
Ganqing	0.01977	0.00086	0.868488	0.544212	0.184973	1.6676	0.012849	1.6689	Pass	0.412	1.53	Pass
South China	−0.00626	−0.00420	0.489528	0.436399	0.067673	1.7081	0.050938	1.7171	Pass	0.903	2.03	Pass
Weihe	−0.00045	−0.00002	0.559638	0.502929	0.004514	1.6991	0.000196	1.7056	Pass	0.901	1.90	Pass
Yuncheng-Linfen	−0.00073	−0.000004	0.564709	0.415061	0.005492	1.7531	0.000037	1.7823	Pass	0.675	2.62	Pass
Taiyuan-Xinzhou	0.00012	0.000008	0.417594	0.361556	0.001493	1.7139	0.000119	1.7247	Pass	0.862	2.08	Pass
Datong	0.00077	0.000001	0.565184	0.392281	0.009592	1.678	0.000026	1.6802	Pass	0.515	1.62	Pass
North China	−0.00804	−0.00124	0.659720	0.630362	0.100501	1.6656	0.092665	1.6672	Pass	0.957	1.50	Pass

tions, R is the number of undetermined parameters, which can be 3 in the rigid rotation model (Eq. (1)) or 6 (including 3 rotation and 3 strain parameters) in the uniform strain model (Eq. (2)); and $2n - R$ is the degree of freedom of in Eq. (1) or Eq. (2).

If a model is unbiased, the residual between the calculated and the observed value should be close to zero, namely, $\mu_0 = 0$. If Eqs. (1) and (2) are both unbiased, the null hypothesis condition is:

$$H_0: \quad \Delta\bar{v} = \mu_0, \quad H_1: \quad \Delta\bar{v} \neq \mu_0 \tag{7}$$

The T distribution test can be constructed as follows:

$$T = \frac{|\Delta\bar{v} - \mu_0|}{S_{\Delta v}/\sqrt{2n}} \tag{8}$$

Meanwhile, the significance of the difference beweeen two models can be evaluated through an F test. Assuming the variance of Eq. (2) and Eq. (1) are S_1^2 and S_2^2, respectively, and the degree of freedom of the two equtions are f_1 and f_2, respectively, the null hypothesis condition is:

$$H_0: \quad S_1^2 < S_2^2, \quad H_1: \quad S_1^2 \geq S_2^2 \tag{9}$$

The F test value is constructed as follows:

$$F = \frac{S_1^2/f_1}{S_2^2/f_2} = \frac{S_1^2 f_2}{S_2^2 f_1} \tag{10}$$

The results of T and F tests are shown in Table 1 at a significance level $\alpha = 0.05$. The results of the T tests for both Eqs. (1) and (2) satisfy the requirements of the unbiasedness of hypothesis test (Table 1).

It can be seen from Table 1 that the average residuals for the two models are all close to zero. However, Table 1 shows that the absolute average residual based on Eq. (2) is obviously less than that from Eq. (1) and that the variance of Eq. (2) is less than that of Eq. (1) under the significance level of $\alpha = 0.05$, if assumed $S_1^2 < S_2^2$. Therefore, it is better to use Eq. (2) to describe the crustal deformation characteristic for most blocks at the Fenwei basin and its surroundings. For the Ordos block, the absolute value of the average residual is about 0.007 for the rigid block model (Eq. (1)), but about 0.009 for the rigid rotation and homogeneous strain model (Eq. (2)). This signifys that the Ordos block has an obviously rigid feature and the rigid block model (Eq. (1)) is suitable to describe the crustal deformation feature of the block. We then skip the following tests for the Ordos block.

4.2. Significance test of strain parameters of models

The rigid rotation and homogeneous strain model (Eq. (2)) can be expressed in a matrix form as follows:

$$\underset{2\times1}{V} = \underset{2\times3}{A}\,\underset{3\times1}{X} + \underset{2\times3}{B}\,\underset{3\times1}{Y} \tag{11}$$

where

$$A = \begin{bmatrix} -r\sin\varphi\cos\lambda & r\sin\lambda \\ -r\sin\varphi\sin\lambda & -r\cos\lambda \\ r\cos\varphi & 0 \end{bmatrix}^T, \quad X = \begin{bmatrix} \omega_x \\ \omega_y \\ \omega_z \end{bmatrix} \tag{12}$$

$$B = \begin{bmatrix} r(\lambda-\lambda_0)\cos\varphi & 0 \\ r(\varphi-\varphi_0) & r(\lambda-\lambda_0)\cos\varphi \\ 0 & r(\varphi-\varphi_0) \end{bmatrix}^T, \quad Y = \begin{bmatrix} \varepsilon_e \\ \varepsilon_{en} \\ \varepsilon_n \end{bmatrix} \tag{13}$$

Eq. (11) can be regarded as a linear model. The main parameters of the model are Euler vector X and strain parameters Y.

Eq. (11) can be rewriten as follows by applying the method of linear hypothesis testing (Koch, 1980; Tao, 2007):

$$\begin{cases} \Delta_{2n\times1} = \bar{A}\begin{bmatrix} X_{3\times1} \\ Y_{3\times1} \end{bmatrix} - l, \quad \bar{A} = (A_{2n\times3}, B_{2n\times3}) \\ H\begin{bmatrix} X \\ Y \end{bmatrix} = 0, \quad H = (0_{3\times3}, I_{3\times3}) \end{cases} \tag{14}$$

where the linear hypothesis is $H_0: Y = 0$, Δ is the residual error of the velocity component, $l = \begin{bmatrix} V_e \\ V_n \end{bmatrix}$, n is the number of GPS station in the study region, I is the identity matrix.

After H_0 is set up, the F test is constructed as:

$$F = \frac{R/rank(H)}{T/(2n - rank(\bar{A}))} \sim F_{(rank(H),\,2n-rank(\bar{A}))} \tag{15}$$

Namely,

$$\frac{\hat{Y}^T Q_{\hat{Y}\hat{Y}}^{-1}\hat{Y}/3}{T/(2n-6)} \sim F_{(3,2n-6)} \tag{16}$$

The reject region is:

$$F > F_{(\alpha,3,2n-6)} \tag{17}$$

where $rank(\cdot)$ in Eq. (15) is the rank of H, $Q_{\hat{Y}\hat{Y}}^{-1}$ in Eq. (16) is the inverse of the weighting matrix for $\hat{Y}$, T in Eq. (16) is the sum of residual squares, and α in Eq. (17) is the given significance level.

The F test reflects the proportion between the local interior deformation and the rigid motion of the block, which should be a smaller value if the interior deformation is insignificant. Therefore, if H_0 is rejected under a significance level of α, it is reasonable to consider that the strain parameters are significant. Accordingly, the interior deformation within the block should not be ignored. If H_0 is accepted, namely, Eq. (17) is false, we are conviced that the strain parameters are not significant. So we do not need to take into account the interior deformation within the block and can consider the block as a rigid one. Using the GPS observations in the study

Table 2
Significance tests of strain parameters of the Fenwei basin and its surrounding blocks.

Blocks (basins) name	*F* value	Reference critical value (significance level is 0.05)	Results
Yinchuan	10.593	3.49	Reject
Hetao	2.871	3.24	Accept
Yinshan	2.817	3.49	Accept
Ganqing	34.468	2.76	Reject
South China	2.953	3.05	Accept
Weihe	3.303	2.98	Reject
Yuncheng-Linfen	5.255	3.49	Reject
Taiyuan-Xinzhou	3.561	3.1	Reject
Datong	17.854	2.82	Reject
North China	3.066	2.74	Reject

area, we have conducted linear hypothesis tests to determine the significance of strain parameters. The results are shown in Table 2.

It can be seen from Table 2 that the the null hypothesis can be accepted for Hetao, Yinshan and South China blocks. Therefore, there is no need to introduce strain parameters when establishing the deformation models of these blocks under a significance level of $\alpha = 0.05$. Therefore, these 3 blocks along with the Ordos block can be represented by a rigid block model (Eq. (1)). However, the *F* values for other blocks are larger than the reference critical value, indicating that the interior deformation within these blocks is relatively significant. Thus, the interior strain parameters have to be considered when establishing the deformatiom models of these 7 blocks.

4.3. Homogeneous strain condition testing

The hypothesis condition of establishing the model expressed by Eq. (2) is that the interior strain of the block is homogeneous. If this is true, we can use the model (Eq. (2)) to study the homogeneous strain characteristic of the block. But if not, the deformation model should have not only the first term of the strain parameters, but also the quadratic terms of the strain parameters expressed in Eq. (4). In addition, we must consider whether all or some of the quadratic terms of the strain parameters have to be introduced. Our testing procedures are summarized below.

The GPS velocity of any point can be considered as the sum of three velocity parts, namely (Huang and Guo, 2003):

$$V_i = V_{ri} + V_{ui} + V_{li} \tag{18}$$

where V_i is the velocity component of any GPS station (i), V_{ri} is the velocity component caused by the rigid rotation of the block (e.g., Eq. (1)), V_{ui} is the velocity component caused by the homogeneous strain within the block (e.g., Eq. (2)), and V_{li} is the velocity component caused by the inhomogeneous strain within a block. Our next goal is to test whether the internal strain within a block has uneven characteristics based on the V_{li} velocity component.

The Euler vector of each block can be obtained based on the Euler rotation theorem, which can be used to estimate the V_{ri} component. Then the remaining velocity component that excludes the movement of rigid block rotation is achieved, namely, $V_{1i} = V_i - V_{ri}$.

Table 4
Significance tests of the quadratic terms of strain parameters of the Fenwei basin and its surrounding blocks.

Blocks (basins) name	*F* value	Reference critical value (significance level is 0.1)	Results
Ganqing	3.675	1.89	Significant
Weihe	2.767	2.09	Significant
Yuncheng-Linfen	0.324	3.05	Not significant
Taiyuan-Xinzhou	2.625	2.24	Significant
Datong	2.231	1.95	Significant
Nouth China	2.559	1.88	Significant

By applying this equation into Eq. (2), we can further obtain the velocity component that deducts the deformation due to the homogenous strain within a block, namely, $V_{2i} = V_i - V_{ri} - V_{ui}$, which is caused by the local deformation (i.e., inhomogeneous strain). Finally, based on the relationship between the displacement and strain within a two-dimensional plane, it is possible to calculate the local strain parameters and their standard deviations. Then we assign a 2-sigma ($\alpha = 0.05$) threshold for statistical significance testing to decide whether the strain parameter is statistically significant.

Based on the above procedure, if the calculated local strain parameters are not significant, the deformation within a block is homogeneous. The hypothesis condition of Eq. (2) is then reasonable for studying the crustal deformation charateristic of the block. Otherwise we have to introduce the quadratic terms of strain parameters to allow for the inhomogeneous strain within the block. The calculated local strain rate and its standard deviation of each block are shown in Table 3.

Based on strain parameters and their standard deviations (Table 3) and a 2-sigma ($\alpha = 0.05$) threshold, we have conducted statistical significance testing for strain parameters of all blocks. We have found that strain parameters are significant for all blocks except Yinchuan block, suggesting that strain is homogeneous within Yinchuan block and inhomogeneous in others. Therefore, the homogeneous strain model (Eq. (2)) is adequate to characterize the deformation characteristics of Yinchuan block. Therefore, for the other blocks (Ganqing block, Weihe, Yuncheng-Lingfen, Taiyuan-Xinzhou and Datong basins, and North China block), we have to introduce the quadratic terms of strain parameters to establish the kinematic model as expressed by Eq. (4).

Furthermore, we need to conduct hypothesis testing about whether the introduced quadratic terms of strain parameters can fully represent the uneven deformation nature of the blocks. Empolying the same procedure for linear model hypothesis testing in Section 4.2, we should test the statistical significance of the quadratic terms of strain parameters in Eq. (4). The number of quadratic terms of the strain parameters is 6, and the corresponding degree of freedom is $(6, 2n - 12)$. Under a significance level of $\alpha = 0.1$, the test results are shown in Table 4.

It can be seen from Table 4 that the quadratic terms of the strain parameters of the Ganqing and North China blocks, Weihe, Taiyuan-Yizhou and Datong basins are significant under a significance level

Table 3
Results of strain homogeneity of the Fenwei basin and its surrounding blocks (unit of 1×10^{-9}/yr).

Blocks (basins) name	$\varepsilon_e \pm \Delta\varepsilon_e$	$\varepsilon_{en} \pm \Delta\varepsilon_{en}$	$\varepsilon_n \pm \Delta\varepsilon_n$	$\omega \pm \Delta\omega$	(2-Sigma) testing
Yinchuan	−8.4 ± 3.8	2.9 ± 2.6	−1.1 ± 1.0	3.2 ± 2.3	Accept
Ganqing	27.4 ± 2.4	−6.3 ± 0.68	1.3 ± 1.1	15.5 ± 1.1	Reject
Weihe	63.2 ± 0.7	65.6 ± 3.7	−87.9 ± 1.9	76.3 ± 1.9	Reject
Yuncheng-Linfen	−287.1 ± 2.9	−42.5 ± 0.001	20.1 ± 1.5	−192.4 ± 1.6	Reject
Taiyuan-Xinzhou	14.9 ± 3.6	−2.3 ± 1.9	29.1 ± 1.8	5.3 ± 1.8	Reject
Datong	2.6 ± 1.2	2.7 ± 1.5	−10.9 ± 1.0	−3.5 ± 1.1	Reject
North China	−13.5 ± 2.1	−1.7 ± 0.6	17.6 ± 0.9	−1.6 ± 0.9	Reject

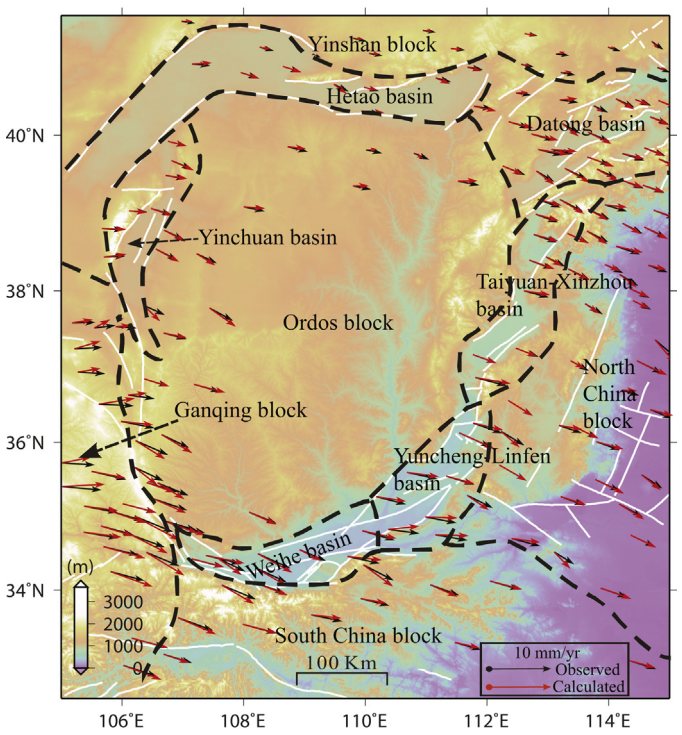

Fig. 3. Comparison of the observed GPS velocities (black arrows) and the predicted velocities (red arrows) based on our kinematic block model. (For interpretation of the references to color in this figure legend, the reader is referred to the web version of the article.)

of $\alpha = 0.1$, indicating that the introduced quadratic terms of strain parameters can reasonably reflect the uneven deformation characteristics of these blocks (Eq. (4)). Meanwhile, by applying the method of linear model testing, we proceed to conduct significance tests on each of the quadratic terms of the strain parameters one after another. The results show that all quadratic terms of the strain parameters in Eq. (4) are significant for these 5 blocks.

However, the test result for the Yuncheng-Linfen basin is not significant under the same significance level (Table 4). Then we apply the above-mentioned method to determine the number of quadratic terms required for the Yuncheng-Linfen basin. Finally, we have determined that the deformation model for the Yuncheng-Linfen basin can expressed as follows:

$$\begin{bmatrix} V_e \\ V_n \end{bmatrix} = \begin{bmatrix} -r\sin\varphi\cos\lambda & -r\sin\varphi\sin\lambda & r\cos\varphi \\ r\sin\lambda & -r\cos\lambda & 0 \end{bmatrix} \begin{bmatrix} \omega_x \\ \omega_y \\ \omega_z \end{bmatrix} + \begin{bmatrix} A_0 & B_0 \\ B_0 & C_0 \end{bmatrix} \begin{bmatrix} x \\ y \end{bmatrix} + \frac{1}{2} \begin{bmatrix} \xi_1 \\ \zeta_1 \end{bmatrix} x^2 + \begin{bmatrix} \xi_3 \\ \zeta_3 \end{bmatrix} xy \quad (19)$$

Finally, the plate kinematic models, which can reflect the deformation characteristics of each blocks of the Fenwei Basin and its surroundings, are obtained through hypothesis.

The results can be summarized as follows:

- It is reasonable to apply the rigid block model (Eq. (1)) to fit the strain feature of the Ordos, South China and Yinshan blocks and the Hetao Basin.
- Eq. (2) is suitable for the Yinchuan basin.
- Eq. (4) is suitable for the Ganqing block in the eastern margin of Tibetan Plateau, the North China block, the Weihe, Taiyuan-Xinzhou and Datong basins.
- Eq. (19) is suitable for the Yuncheng-Linfen basin.

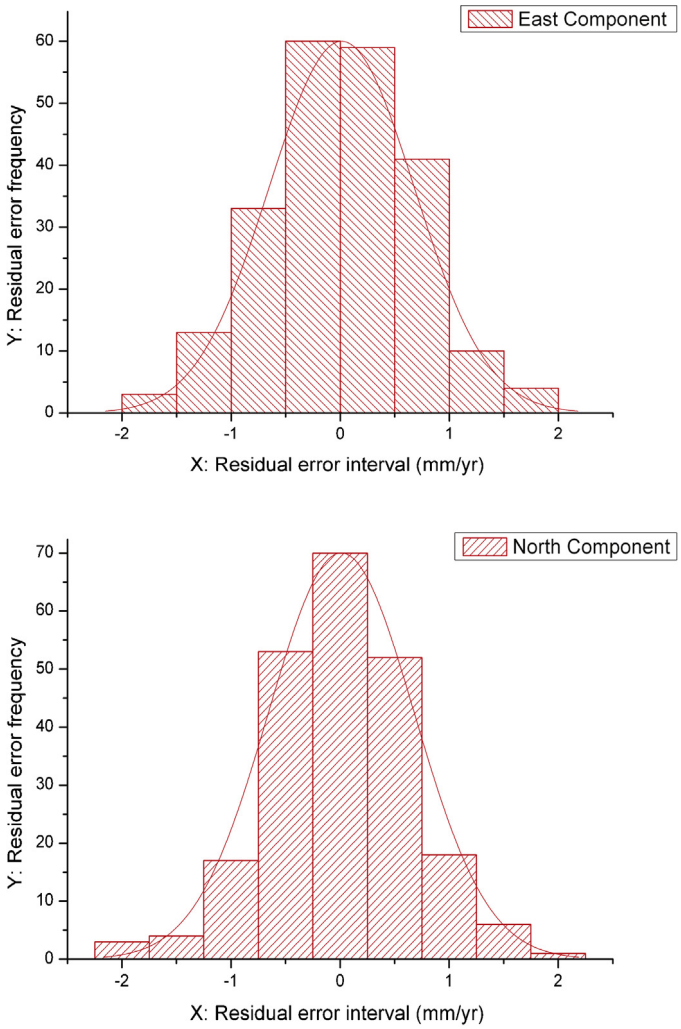

Fig. 4. Histogram of residuals between the observed and model-predicted velocities in the east and north components.

5. Results and discussion

Based on GPS data from the CCMON, we have obtained the parameters of crustal deformation characteristics based on our plate kinemataic model for the 11 blocks over the Fenwei basin. Fig. 3 shows the comparison between the observed GPS velocity and the model-prediciton, and Fig. 4a and b presents histograms of residuals between the observed and the model-predicted GPS velocities. It can be seen from Fig. 4 that residuals approximately obey the normal distribution, suggesting the model does not have any systematic error.

The vector map of the principal strain rate and the contour map of the maximum shear strain rate are also constructed based on the strain eigenvalues (Figs. 5 and 6).

As can be seen from Fig. 5, tensile strain in the NW–SE direction dominates most of the Fenwei basin, particularly over the middle of the Weihe basin and the whole Shanxi graben. The tensile strain rate is generally higher than 2.8×10^{-8}/yr. The western part of the Weihe basin is in a state of slight compression while the middle and eastern parts show tension. The whole Weihe basin shows a state of left-lateral shearing. In addition, the whole Shanxi graben also exhibits tensile strain in the NW–SE direction. Unlike the Weihe basin, the Shanxi graben shows a state of right-lateral shearing.The above analysis indicates that the whole Fenwei basin is significantly influenced by the tectonic stress in the NW–SE direction. The Ganqing block in the eastern margin of Tibet

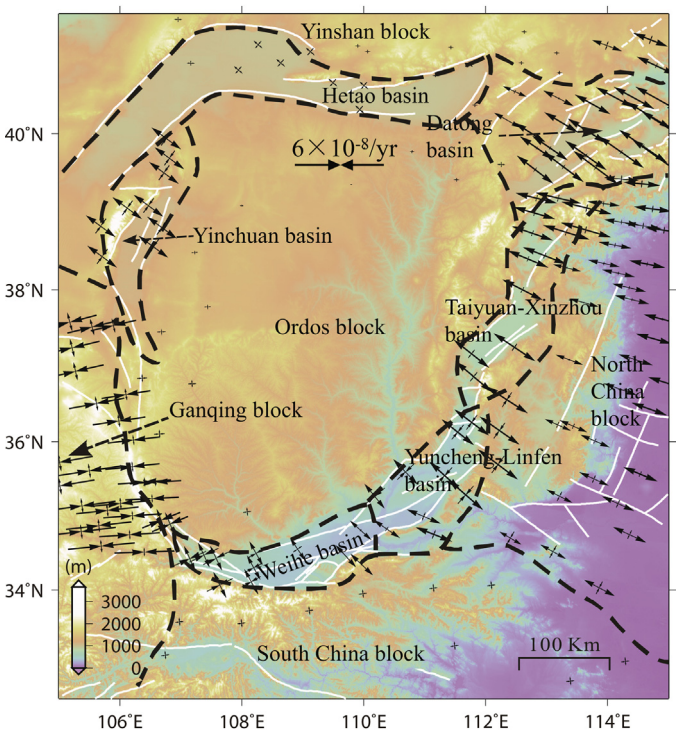

Fig. 5. Vector map of principal strain rates of the Fenwei basin and its surrounding blocks (unit: 10^{-8}/yr).

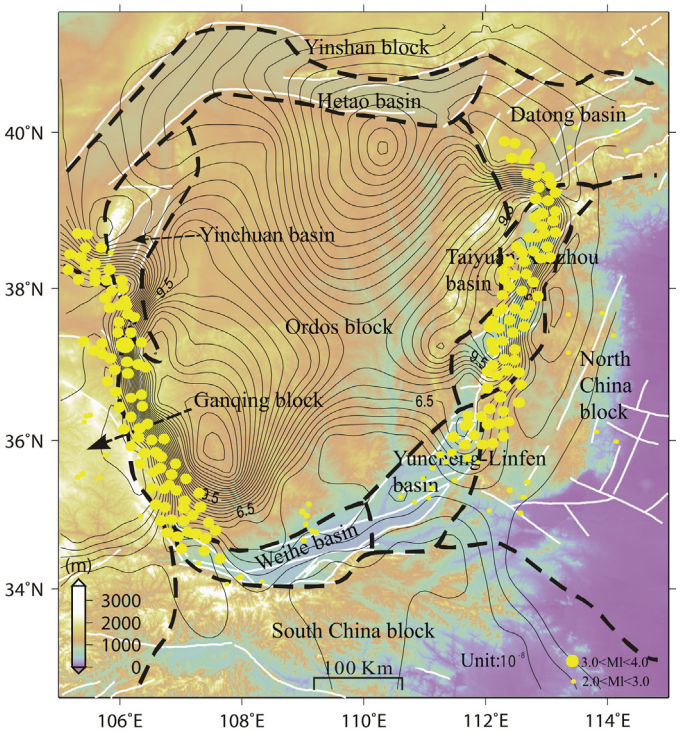

Fig. 6. Contour map of maximum shear strain rates of the Fenwei basin and its surrounding blocks. Yellow dots represent shallow earthquakes with local magnitues (ML) between 2.0 and 4.0 for the period of 1999–2007. (For interpretation of the references to color in this figure legend, the reader is referred to the web version of the article.)

presents distinct compressive strain in the E-W direction with a mean strain rate reaching -3.8×10^{-8}/yr. The Yinchuan basin presents tensile strain in the NW–SE direction, with a value higher than 2.8×10^{-8}/yr. The whole North China block mainly shows tensile strain in the NW–SE direction, with a mean value reaching 3.5×10^{-8}/yr. In addition, the direction of the principal tensional strain orients at an azimuth angle of about 275° from the north over the northern part of the North China block, while it directs to about 300° from the north in the southern part (Fig. 5). Therefore the North China block exhibits characteristics of clockwise rotation to some extent. The South China, Ordos, and Yinshan blocks and the Hetao basin all show characteristics of rigid block rotation.

As can be seen from Fig. 6 the boundaries of the Ganqing and Ordos blocks as well as the Shanxi graben are the regions possessing the maximum shearing stain (larger than 9.5×10^{-8}/yr). The magnitude of the shearing strain reflects the degree of the crust deformation; the higher the shearing strain, the more severe the tectonic activity. Hence, the tectonic activity of the above region is significant, which is supported by the fact that this region is an earthquake-prone zone (Fig. 6) (Fan et al., 2003; Wang, 2009; Zhang et al., 2005).

6. Conclusions

In this paper, we have established different types of regional plate kinematic models based on GPS data. After examining these models using three steps of statistical significance tests, we have obtained the present-day deformation characteristic of the Fenwei basin and its surroundings: (a) Ordos, South China and Yinshan blocks, and Hetao basin deform rigidly; (b) Yinchuan basin has a homogeneous strain; and (c) Ganqing and North China blocks, and Weihe, Yuncheng-Linfen, Taiyuan-Xinzhou and Datong basins have inhomogeneous strain.

Our results indicate that the overall principal strain of Fenwei basin is mainly tensile in the NW–SE direction. This is consistent with the recent crustal deformation features over the region. For example, it has been proposed that the extensional (NW–SE) grabens and rift basins in East Asia are the result of the northwesternward subduction of the Pacific plate and the far-field effect of the India-Eurasia collision (Liu et al., 2007; Schellart et al., 2007; Hintersberger et al., 2010; White and Lister, 2012), either through eastward slab rollback (Schellart and Lister, 2005; Schellart et al., 2007; Royden et al., 2008) or due to a reduction in Pacific-Eurasia plate convergence (Northrup et al., 1995; Hall et al., 2003). Furthermore, many publications have confirmed that Cenozoic NW–SE extension existed in Eastern China, including the Fenwei basin (e.g., Zhang et al., 2003; Wang et al., 2012; Mercier et al., 2013).

Our results of plate kinematic models of Fenwei basin can provide important insights into understanding the recent crustal deformation and geodynamics of East Asia and the mechanism of frequent geological disasters in Fenwei basin.

The accuracy of a kinematic model of crustal deformation depends on the availability of GPS observations. The density of GPS data over much of Fenwei basin and its surrounding is suitable for establishing a regional plate kinematic model. In areas where GPS data are relatively sparse (e.g., northwestern part of Yinchuan basin and southwestern part of Hetao basin), our solutions might have room to improve. In the future, we expect to be able to better constrain the regional plate kinematic model by combining GPS observations, interferometric synthetic aperture radar imagery, and gravity measurement.

Acknowledgements

This study is supported by Nature Science Fund of China (NSFC) (project nos: 41202189, 41274005 and 41104019), China

Postdoctoral Science Foundation funded project (2013M530412), and a Key Project of the Ministry of Land & Resources, China (project no: 1212010914015). Part of this work was carried out at the University of Glasgow, which was supported by the Natural Environmental Research Council (NERC) through the GAS project (Ref: NE/H001085/1) and was also supported in part by a China 863 Project (ID: 2009AA12Z317). Some figures were prepared using the public domain GenericMapping Tools GMT (Wessel and Smith, 1998). Finally, we thank the very constructive comments and suggestions from the editor-in-chief, reviewer N. Shestakov, and an anonymous reviewer.

References

Argus, D.F., Gordon, R.G., Heflin, M.B., Ma, C., Eanes, R.J., Willis, P., Peltier, W.R., Owen, S.E., 2010. The angular velocities of the plates and the velocity of the Earth's center from space geodesy. Geophysical Journal International 18, 1–48.

Argus, D.F., Gordon, R.G., DeMets, C., 2011. Geologically current motion of 56 plates relative to the no-net rotation reference frame. Geochemistry, Geophysics, Geosystems 12.

Altamimi, Z., Collilieux, X., Legrand, J., et al., 2007. ITRF2005: a new release of the International Terrestrial Reference Frame based on time series of station positions and Earth Orientation Parameters. Journal of Geophysical Research: Solid Earth 112 (B9), B9401.

Burbidge, D.R., 2004. Thin plate neotectonic models of the Australian plate. Journal of Geophysical Research: Solid Earth (1978–2012) 109 (B10).

Chang, X., Liu, Y.K., He, J.K., Sun, H.C., 2007. Lower velocities beneath the Taihang Mountains, Northeastern China. Bulletin of the Seismological Society of America 97, 1364–1369.

Drewes, H.,2009. The actual plate kinematic and crustal deformation model APKIM2005 as basis for a non-rotating ITRF. In: Geodetic Reference Frames. IAG Symposia 134. Springer, pp. 95–99.

DeMets, C., Gordon, R.G., Argus, D.F., 2010. Geologically current plate motions. Geophysical Journal International 181, 1–80.

Dai, W.Q., Ren, J., Zhao, X.M., 2004. Characteristics of horizontal crustal movement in Weihe basin and adjacent zones by GPS observation. Acta Seismologica Sinica 26 (3), 256–260.

Dewey, J.F., Pitman, W.C., William, B.F., Bonnon, J., 1973. Plate tectonics and the evolution of the Alpine system. Geological Society of America Bulletin 84 (10), 3137–3180.

Fan, J.X., Ma, J., Gan, W.J., 2003. The motion integration and activity alternating of different orientation boundary of Ordos block. Science in China Series D 33 (Suppl.) (in Chinese).

Fu, Y., Zhu, W., Wang, X., Duan, W., 2002. Present-day crustal deformation in china relative to ITRF97 kinematic plate model. Journal of Geodesy 76 (4), 216–225.

Huang, L.R., Guo, L.Q., 2003. Global crustal motion deduced from GPS observation. Earth Science Frontiers 10 (Suppl.), 17–21 (in Chinese).

Huang, J.L., Zhao, D.P., 2006. High-resolution mantle tomography of China and surrounding regions. Journal of Geophysical Research: Solid Earth 1111 (B9).

Hintersberger, E., Thiede, R.C., Strecker, M.R., Hacker, B.R., 2010. East–west extension in the NW Indian Himalaya. Geological Society of America Bulletin 122 (9–10), 1499–1515.

Hall, C.E., Gurnis, M., Sdrolias, M., Lavier, L.L., Muller, R.D., 2003. Catastrophic initiation of subduction following forced convergence across fracture zones. Earth and Planetary Science Letters 212, 15–30.

Herring, T.A., 2002. GLOBK: Global Kalman Filter VLBI and GPS Analysis Program, Version 10.0. Massachusetts Institute of Technology, Cambridge.

Jiang, W.L., Xiao, Z.M., Xie, X.S., 2000. Segmentations of active normal dip-slip faults around Ordos block according to their surface ruptures in historical strong earthquakes. Acta Seismologica Sinica 13 (5), 552–562.

Koch, K.R., 1980. Parameterschatzung und hypothesen tests in linearen modellen. Dummler, Bonn.

King, R.W., Bock, Y., 2000. Documentation for the GAMIT GPS Analysis Software, Release 10.0. Massachusetts Institute of Technology, Cambridge.

Li, Y.X., Zhang, J.H., He, J.K., 2007. Current day tectonic motion and intraplate deformation strain field obtained from space geodesy in the Pacific plate. Chinese Journal of Geophysics 50 (2), 437–447 (in Chinese).

Li, Z.H., Feng, W.P., Xu, Z.H., Paul, C., Zhang, J.F., 2008. The 1998 Mw 5.7 Zhangbei-Shangyi (China) earthquake revisited: a buried thrust fault revealed with interferometric synthetic aperture radar. Geochemistry, Geophysics, Geosystems 9 (4.).

Lin, W., Faure, M., Chen, Y., Jia, W.B., Wang, F., Wu, L., Charles, N., Wang, J., Wang, Q.C., 2013. Late Mesozoic compressional to extensional tectonics in the Yiwuluhan massif, NE China and its bearing on the evolution of the Yinshan–Yanshan orogenic belt: Part I: Structural analyses and geochronological constraints. Gondwana Research 23 (1), 54–77.

Liu, M., Yang, Y.Q., Shen, Z.K., Wang, S.M., Wang, M., Wan, Y.G., 2007. Active tectonics and intracontinental earthquakes in China: the kinematics and geodynamics. Geological Society of America Special Papers 425, 299–318.

McKenzie, D.P., 1972. Active tectonics of the Mediterranean system. Geophysical Journal of the Royal Astronomical Society 30 (2), 109–185.

Myers, J.R., Gomez, F.G., 2010. Analysis of Subsidence and Ground Fissuring in the FenWei Basin (Northern China) using Radar Interferometry. AGU Fall Meeting Abstracts#H23F-1297.

Mercier, J.L., Vergely, P., Zhan, Y.Q., Hou, M.J., Bellier, O., Wang, Y.M., 2013. Structural records of the Late Cretaceous–Cenozoic extension in Eastern China and the kinematics of the Southern Tan-Lu and Qinling Fault Zone (Anhui and Shaanxi provinces, PR China). Tectonophysics 582 (2), 50–75.

Nanjo, K.Z., Turcotte, D.L., Shcherbakov, R., 2005. A model of damage mechanics for the deformation of the continental crust. Journal of Geophysical Research: Solid Earth (1979–2012) 110 (B7).

Northrup, C.J., Royden, L.H., Burchfiel, B.C., 1995. Motion of the Pacific plate relative to Eurasia and its potential relation to Cenozoic extension along the eastern margin of Eurasia. Geology 23, 719–722.

Prawirodirdjo, L., Bock, Y., 2004. Instantaneous global plate motion model from 12 years of continuous GPS observations. Journal of Geophysical Research 109, B08405.

Reynolds, S.D., Coblentz, D.D., Hillis, R.R., 2002. Tectonic forces controlling the regional intraplate stress field in continental Australia: results from new finite element modeling. Journal of Geophysical Research 107 (B7), 2131.

Royden, L.H., et al., 2008. The geological evolution of the Tibetan Plateau. Science 321, 1054.

Savage, J.C., Gan, W., Svarc, J.L., 2001. Strain accumulation and rotation in the Eastern California shear zone. Journal of Geophysical Research 106 (B10), 21995–22007.

Shi, Y.L., Zhu, S.B., 2006. Discussion in methods of calculating strain with GPS displacement data. Journal of Geodesy and Geodynamics 26 (1), 2–8 (in Chinese).

Sella, G.F., Dixon, T.H., Mao, A., 2002. REVEL: a model for recent plate velocities from space geodesy. Journal of Geophysical Research 107, B4.

Shen, Z.K., Zhao, C.K., Yin, A., Li, Y.X., David, D.J., Fang, P., Dong, D.N., 2000. Contemporary crustal deformation in east Asia constrained by Global Positioning System measurements. Journal of Geophysical Research: Solid Earth 1105 (B3), 5721–5734.

Schellart, W.P., Lister, G.S., 2005. The role of the East Asian active margin in widespread extensional and strike-slip deformation in East Asia. Journal of the Geological Society 162, 959–972.

Schellart, W.P., Freeman, J., Stegman, D.R., Moresi, L., May, D., 2007. Evolution and diversity of subduction zones controlled by slab width. Nature 446, 308–311.

Tao, B.Z., 2007. The Statistical Theory and Methods of the Survey Measurement Data Processing. Surveying and Mapping Press, Beijing (in Chinese).

Teng, J.W., 2003. Introduction to Solid Earth Geophysics. Seismological Press, Beijing (in Chinese).

Tang, Y.C., Chen, Y.J., Fu, Y.V., Wang, H., Zhou, S., Sandvol, E., Ning, J.Y., Feng, Y.G., Liu, M., 2010. Mantle anisotropy across the southwestern boundary of the Ordos block, North China. Earthquake Science 23 (6), 549–553.

Tian, X.B., Teng, J.W., Zhang, H.S., Zhang, Z.J., Zhang, Y.Q., Yang, H., Zhang, K.K., 2011. Structure of crust and upper mantle beneath the Ordos block and the Yinshan Mountains revealed by receiver function analysis. Physics of the Earth and Planetary Interiors 184, 186–193.

Wang, X.W., Song, M.Q., Yang, G.H., 2010. Research on relationship between stress field variation and earthquakes in Shanxi area, China. Chinese Journal of Geophysics 53 (3), 400–407 (in Chinese).

Wang, M., (Ph.D. thesis) 2009. Analysis of GPS Data with High Precision and Study on Present-day Crustal Deformation in China (in Chinese).

Wessel, P., Smith, W.H.F., 1998. New, improved version of generic mapping tools released. EOS, Transactions American Geophysical Union 79 (47), 579.

Wu, J.C., Tang, H.W., Chen, Y.Q., Li, Y.X., 2006. The current strain distribution in the North China Basin of eastern China by least-squares collocation. Journal of Geodynamics 41, 462–470.

Wang, Q., Zhang, P.Z., Niu, Z.J., Freymueller, J.T., Lai, X.Z., Li, Y.X., Zhu, W.Y., Liu, J.N., Bilham, R., Larson, K.M., 2002. Present-day crustal movement and tectonic deformation in China continent. Science in China Series D: Earth Sciences 45 (10), 865–874.

Wang, K.Y., Ma, J., Diao, G.L., 2012. Presentday stress state of the Shanxi tectonic belt. Geodynamics & Tectonophysics 3 (3), 195–202.

White, L.T., Lister, G.S., 2012. The collision of India with Asia. Journal of Geodynamics (56–57), 7–17.

Yang, M.H., Li, L., Zhou, J., Qu, X.Y., Zhou, D., 2013. Segmentation and inversion of the Hangjinqi fault zone, the northern Ordos basin (North China). Journal of Asian Earth Sciences 70–71, 64–78.

Zhang, P.Z., Gan, W.J., Shen, Z.K., 2005. A coupling model of rigid-block movement and continuous deformation: patterns of the present-day deformation of China's continent and its vicinity. Acta Geologoca Sinica 79 (6), 748–756.

Zhang, Q., Zhu, W.G., Xiong, Y.Q., 1999. Global plate motion models incorporating the velocity field of ITRF96. Geophysical Research Letters 26 (18), 2813–2816.

Zhang, Q., Qu, W., Wang, Q.L., Peng, J.B., Drummond, J., Li, Z.H., Lin, Q., 2011. Analysis of present tectonic stress and regional ground fissure formation mechanism of the Weihe basin. Survey Review 43 (322), 382–389.

Zhang, Y.Q., Ma, Y.S., Yang, N., Shi, W., Dong, S.W., 2003. Cenozoic extensional stress evolution in North China. Journal of Geodynamics 36 (5), 591–661.